 CMES, vol.92, no.1, pp.63-85, 2013

A new implementation of the numerical manifold method (NMM) for the modeling of non-collinear and intersecting cracks

Y.C. Cai[1,2,3], **J. Wu**[2], **S.N. Atluri**[3]

Abstract: The numerical manifold method (NMM), based on the finite covers, unifies the continuum analyses and discontinuum analyses without changing a pre-defined mathematical mesh of the uncracked solid, and has the advantages of being concise in theory as well as being clear in concept. It provides a natural method to analyze complex shaped strong discontinuities as well as weak discontinuities such as multiple cracks, intersecting cracks, and branched cracks. However, the absence of an effective algorithm for cover generation, to date, is still a bottle neck in the research and application in the NMM. To address this issue, a new method for the generation of the finite covers in the NMM is proposed, for the modeling of cracks. In the present algorithm for cover generation, the physical lines such as joints and cracks are described by geometric functions, the mathematical cover is naturally partitioned into different regions by the physical lines, and the regions belonging to a same physical cover, which contains the end points of the physical lines are identified by a simple calculation of the function values of the physical lines. The present method is simple and robust, and is also very fast because it avoids the usage of the complex geometrical algorithms, and the time-consuming judgment of the point-polygon relations, which are commonly used in the previous literature. Several linear elastic fracture problems are analysed here, to demonstrate the validity and the robustness of the proposed algorithms.

Keywords: Finite cover; NMM; Fracture; Crack; Propagation

1 Introduction

An accurate analysis of crack tip fields, and modeling the crack propagation, in a cracked solid, are of vital importance for the safety assessment and life predic-

[1] Corresponding author. Email: yc_cai@163.net.
[2] State Key Laboratory for Disaster Reduction in Civil Engineering, Department of Geotechnical Engineering, Tongji University, Shanghai 200092, P.R.China
[3] Center for Aerospace Research & Education, University of California, Irvine

tion of cracked engineering structures and materials (Atluri 1998, 2005). Because of its simplicity and popularity, the traditional FEM (finite element method) with embedded-singularity elements by [Tong, Pian and Lasry 1973; Atluri, Kobayashi and Nakagaki 1975], singular quarter-point elements by [Henshell and Shaw 1975; Barsoum 1976], and others, has been widely used for fracture modeling with quite a good accuracy, and is adopted in many commercial software such as ANSYS and ABQUS. However, the method finds difficulties in modeling crack propagation, due to a need for a continuous update of the element topology, during crack propagation.

In order to overcome this difficulty, a wide range of new numerical methods, such as the MM (Meshless Methods)[Fleming, Chu, Moran and Belytschko 1997; Xu and Saigal 1998; Belytschko and Fleming 1999;Ching and Batra 2001; Gu, Wang, Zhang and Feng 2011], the NMM (numerical manifold method) [Shi 1991,1992; Ma, An, Zhang and Li 2009], and the XFEM(extended finite element method) [Moes, Dolbow and Belytschko 1999; Sukumar, Chopp, Moes and Belytschko 2001;Sukumar, Chopp, Béchet and Moës 2008], have been developed. They are particularly suitable for fracture modeling, since there is no need for remeshing to accommodate the changing geometry of a crack. Despite clear general progress with these methods, there are still some technical issues in their application to fracture problems, for instance, the complexity in the construction of the discontinuous interpolation functions along the crack, the expense to refine the nodal arrangement near the crack tip, and the complicated algorithm for the subdivision of the integral cells around the crack. More recently, a series of SGBEM (symmetric Galerkin boundary element method)-based methods has been proposed by Atluri and his coworkers [Nikishkov, Park and Atluri 2001; Han and Atluri 2002,2003; Dong and Atluri 2012,2013a,2013b] for modeling complex structures with stationary or propagating cracks. As can be seen from these papers, the SGBEM-based methods are very accurate for computing SIFs (stress intensity factors), require minimal effort for modeling the non-collinear/non-planar propagation of cracks, and require significantly coarser and lower-quality meshes than in other methods, and are probably the best methods so far, for fracture and fatigue analyses.

As a particular method which unifies the continuum analyses, and discontinuum analyses, the NMM proposed by Shi (1991, 1992) has also attracted much interest from researchers in recent years [An, Ma, Cai and Zhu 2011a,2011b; Jiang, Zhou and Li 2009; Liu, Chang, Yang, Wang and Guan 2011; Ma, An, Zhang and Li 2009; Ma, An, and He 2010; Ning, An and Ma 2011; Terada and Kurumatani 2005; Wu and Wong 2012; Zhang, Li, An and Ma 2010; Zhang, Zhang and Yan 2010; Cai, Zhuang and Zhu 2013]. In the NMM, the mathematical mesh of the uncracked solid, regardless of the existence of physical lines of material and ge-

ometric discontinuity (joints and cracks), is first constructed with a defined interpolation accuracy, and the independent local crack functions are augmented in the physical covers, which are obtained from the mathematical covers of the uncracked solid, as cut by the physical lines (joints and cracks). It provides a natural solution, by using the mathematical and physical cover systems, to accommodate problem domains with strong discontinuities as well as weak discontinuities, making itself particularly suitable for dealing with multiple cracks, intersecting cracks, branched cracks or other discontinuities. In the NMM, the generation of the finite covers (different influence domains) constitutes a key and essential part of the NMM theory. However, to the authors' knowledge, the absence of an effective algorithm for cover generation, to date, is still a bottle neck in the research and application in the NMM. To address this issue, a simple, fast and robust cover generation method, and algorithm, is developed, for the modeling of crack problems in this paper. Several stationary linear elastic fracture problems are analysed, to demonstrate the validity and the robustness of the proposed method.

2 Introduction of the basic theory of the NMM

Consider an arbitrary two-dimensional analysis domain Ω as shown in Fig.1. There are three preexisting cracks (chosen as straight lines in this illustration, but can be general lines of discontinuity) represented by the lines denoted as 1, 2 and 3, respectively. In NMM, a material or geometric discontinuity, such as joint or crack, is called a physical line [Shi 1991,1992; Cai, Zhuang and Zhu 2013].

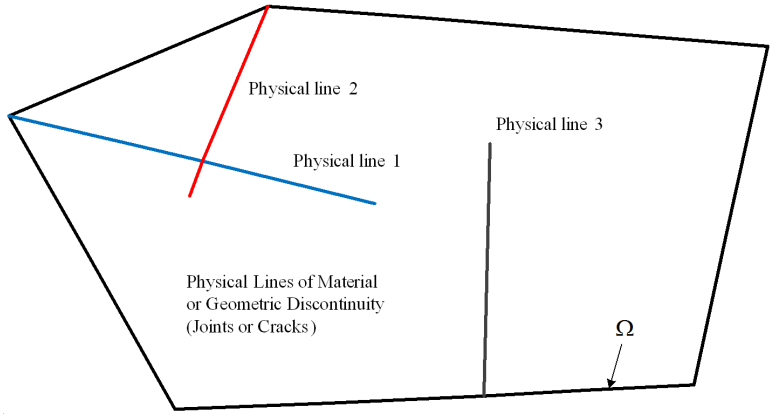

Figure 1: An arbitrary analysis domain with three physical lines (Lines of Material or Geometric Discontinuity, i.e., Joints or Cracks)

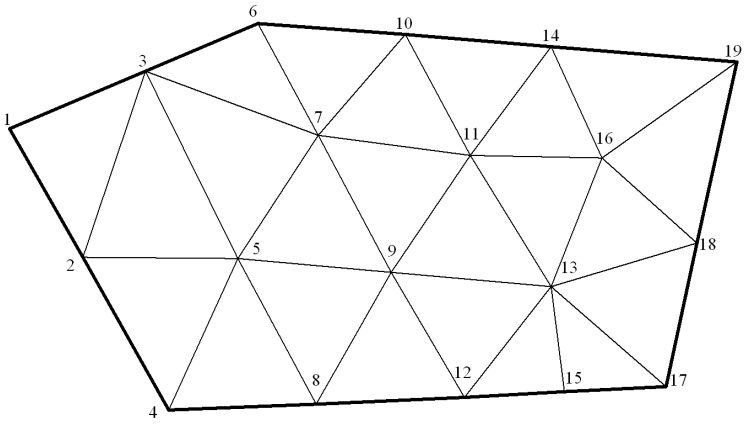

Figure 2: A mathematical mesh for the uncracked domain Ω

In the NMM, two types of separated finite covers ("influence domains"), named as "mathematical covers" and "physical covers", are defined to unify the continuum analysis and discontinuum analysis, respectively. We describe the generation of the finite covers as follows:

(1) Mesh the uncracked problem domain using a triangular mesh [or quadrilateral mesh] following the same procedure in the FEM as shown in Fig.2. The triangular mesh can be used as the mathematical mesh in the NMM. In this step, it is not necessary to consider the existence of physical lines when creating the mathematical mesh. Thus a mathematical mesh is simply the mesh in a domain without a material or geometric discontinuity, i.e., Joints or Cracks.

(2) Add the physical lines to the mathematic mesh, and partition the mathematical element into the "physical elements" by the physical lines. As shown in Fig.3, the mathematical element 3-5-7 is partitioned into "physical elements" (or manifold elements) 3-21-24, 22-7-24-21 and 21-5-22 by the "physical lines" 1 and 2.

(3) Define the mathematical covers ("influence domains") for the mathematical elements. For each node *i*in the mathematical mesh in Fig.2, a mathematical cover centering the node *i* is defined as a polygon composed of all mathematical elements having the node *i*as its vertex. For example, in Fig.4, the mathematical cover 3 is the polygon bounded by 1-2-5-7-6-3, the mathematical cover 5 is the polygon bounded by 2-4-8-9-7-3, and the mathematical cover 7 is the polygon bounded by 3-5-9-11-10-6. Thus, the mathematical cover of node *i* may be considered to be the "Domain of Influence" of node *i*, in the domain without the "physical lines". The intersection of the mathematical covers is the mathematical element, e.g., the

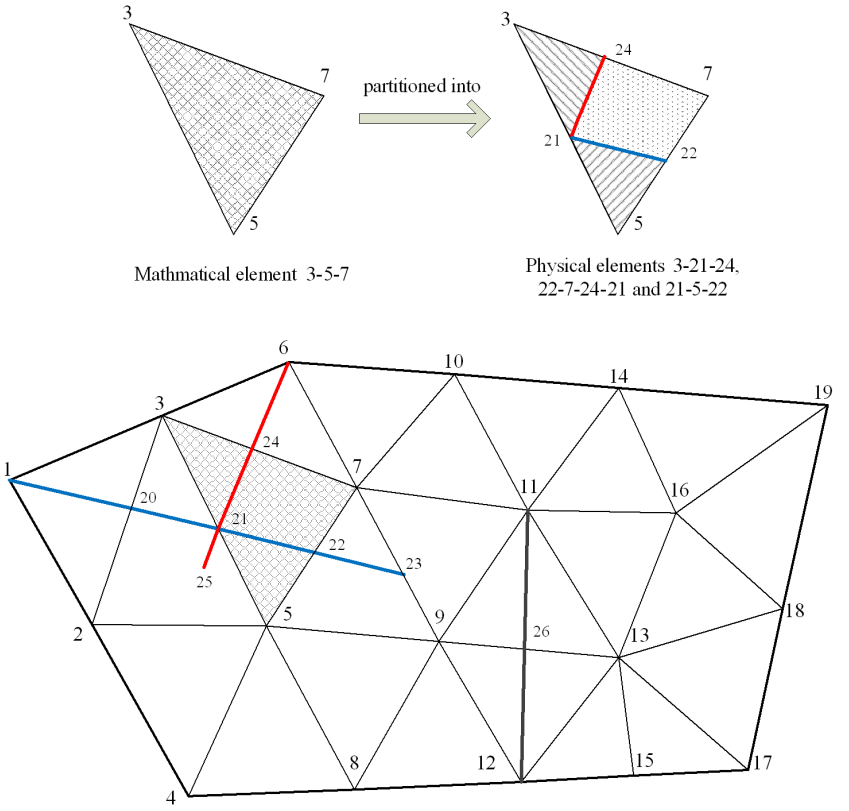

Figure 3: Physical elements for domain Ω

overlap of mathematical covers 3, 5 and 7 forms the mathematical element 3-5-7.

(4) The mathematical covers are further partitioned into physical covers by the physical lines. As shown in Fig.5, the mathematical cover 3 [influence domain of node 3] is partitioned into physical covers 3_1, 3_2 and 3_3, the mathematical cover 5 is partitioned into physical covers 5_1, 5_2 and 5_3, and the mathematical cover 7 is partitioned into physical covers 7_1, and 7_2. Thus, we can see that the physical element 3-21-24 is the overlap part of the three physical covers 3_1, 5_3 and 7_2 the physical element 22-7-24-21 is the overlap part of the three physical covers 3_3, 5_2 and 7_1, and the physical element 21-5-22 is the overlap part of the three physical covers 3_2, 5_1 and 7_1

With the definition of the mathematical covers and physical covers, the interpolation of field variables over each physical element [affected by physical lines] can be easily constructed through the following process. Taking the physical element

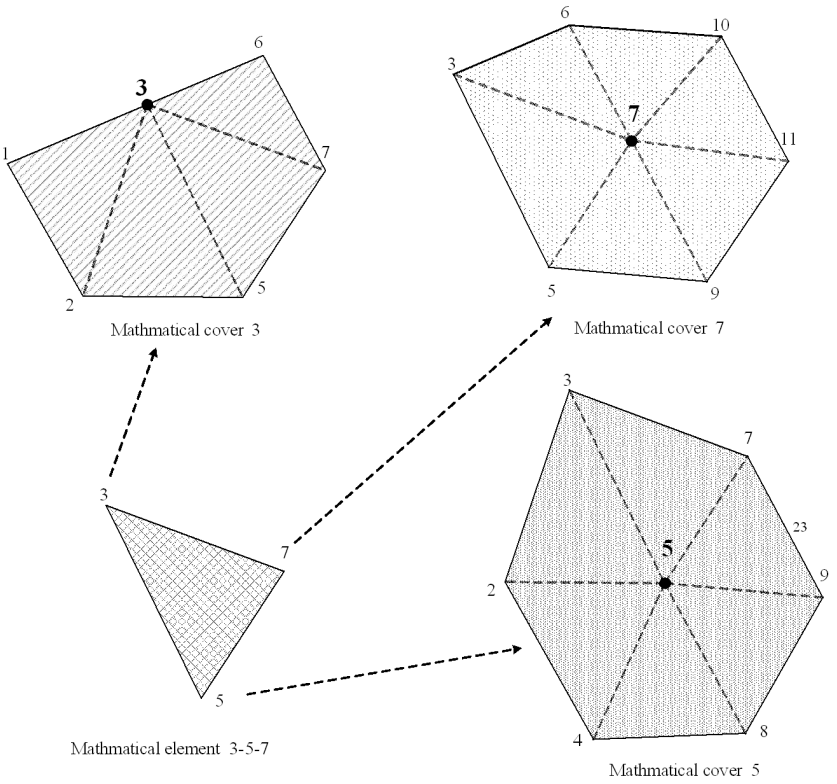

Figure 4: Mathematical covers [influence domains] for mathematical element 3-5-7

22-7-24-21 in Fig.4 belonging to the mathematical element 3-5-7 as an example, the "global" interpolation over the physical element 22-7-24-21 in $x$direction is expressed as

$$u(x,y) = \left[\begin{array}{ccc} w_3 & w_5 & w_7 \end{array} \right] \left\{ \begin{array}{c} u_{3_3}(x,y) \\ u_{5_2}(x,y) \\ u_{7_1}(x,y) \end{array} \right\} \tag{1}$$

where $u_{3_3}(x,y)$,$u_{5_2}(x,y)$ and $u_{7_1}(x,y)$ are the local cover functions defined over the *physical covers* 3_3, 5_2 and 7_1 (Fig.5) respectively, and w_3,w_5 and w_7 are the weight functions over the *mathematical element* 3-5-7 for the three nodes respectively where the subscripts of the weight functions indicates the number of the mathematical node. Note here that the local cover functions $u_i(x,y)$ are defined in the "regions of physical covers", whereas, by comparison, the nodal degrees of freedom or the nodal unknown enrichment parameters are defined at the nodes in

the FEM/XFEM. As can be seen, both the NMM interpolation and the XFEM interpolation have the similar mathematical expression, and can be regarded as the types of partition of unity interpolations (Melenk and Babuska 1996). However, they are derived from the different theories (e.g. the NMM constructs the interpolation based on the finite cover theory and the XFEM constructs the interpolation based on an enrichment function of Heaviside type), and thus they have the different numerical performances when solving various problems. Please refer to An, Fu and Ma (2012) for more comparisons between the NMM and the XFEM.

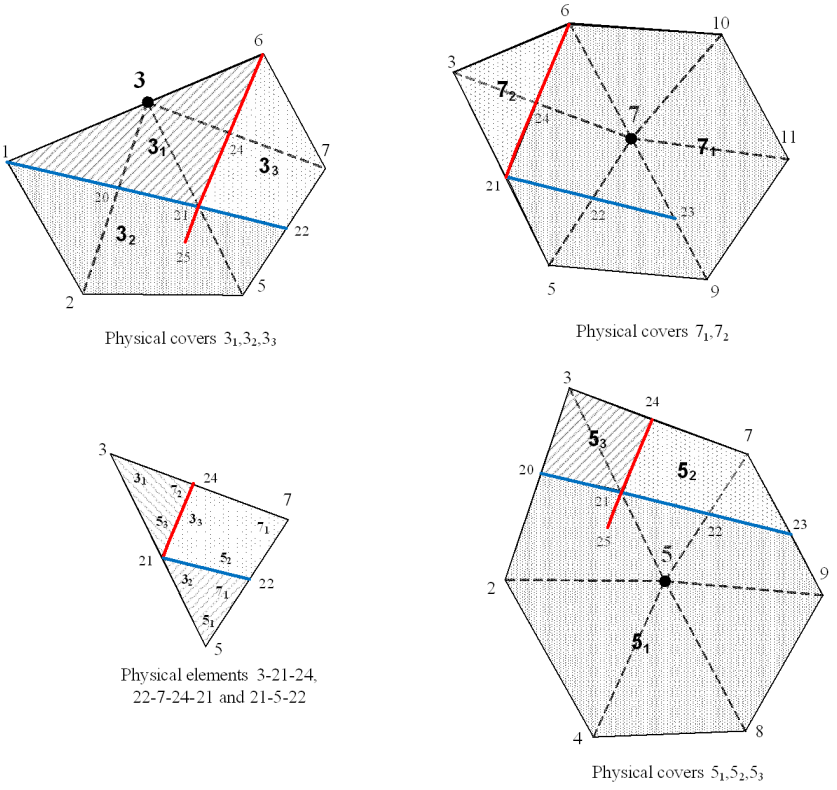

Figure 5: Physical covers and physical elements

The local cover functions $u_{3_3}(x,y)$,$u_{5_2}(x,y)$ and $u_{7_1}(x,y)$ in Eq.(1) can be chosen as the polynomial function or any other functions that reflect the local characteristics of the solution, with the form as

$$u_i(x,y) = \mathbf{H}_i \mathbf{D}_i \tag{2}$$

where $\mathbf{D}_i = \left[\begin{array}{cccc} d_{i1} & d_{i2} & \cdots \end{array} \right]^T$ are the generalized degrees of freedom over physical cover C_i and $\mathbf{H}_i$ is the basis function. In this study, we take $\mathbf{H}_i = [1]$ for common physical covers and $\mathbf{H}_i = \left[\begin{array}{cccc} 1 & \sqrt{r}\sin\frac{\theta}{2} & \sqrt{r}\cos\frac{\theta}{2} & \sqrt{r}\sin\frac{\theta}{2}\sin\theta & \sqrt{r}\cos\frac{\theta}{2}\sin\theta \end{array} \right]$ for the physical covers near a crack tip, where (r,θ) is the local coordinate system at the crack tip. The J integral is used to compute the stress intensity factors (SIFs) over the crack tip.

The weight functions w_3,w_5 and w_7 in Eq.(1) are calculated by

$$w_i = \frac{1}{2A}(a_i + b_i x + c_i y) \tag{3}$$

$$a_i = x_j y_m - x_m y_j,\ b_i = y_j - y_m,\ c_i = -x_j + x_m \tag{4}$$

in which, A is the area of the triangular mathematical element 3-5-7, and $i = 3,5,7$; $j = 5,7,3$; $m = 7,3,5$.

We see that, the global function in Eq.(1) is actually constructed, by multiplying the weight functions $w_i(x,y)$ from the mathematical mesh, with the local functions $u_i(x,y)$ from the physical covers which are obtained from the mathematical covers cut by physical lines (cracks or joints). When there is no physical line involved in a physical element and the local function is taken as $u_i(x,y) = d_{i1}$, the interpolation in Eq.(1) is reduced to the general FEM triangular interpolation.

Similarly the displacement function over physical element 3-21-24 in Fig.5 in $x$direction is expressed as

$$u(x,y) = \left[\begin{array}{ccc} w_3 & w_5 & w_7 \end{array} \right] \left\{ \begin{array}{c} u_{3_1}(x,y) \\ u_{5_3}(x,y) \\ u_{7_2}(x,y) \end{array} \right\} \tag{5}$$

The interpolation over the physical element in y direction can be defined following an identical process.

By comparing Eq. (1) with Eq. (5), it can be found that same weight functions w_2, w_5 and w_7 are used for the physical elements 22-7-24-21 and 3-21-24 in Fig. 5. However as the physical covers 3_3, 5_2 and 7_1 of the physical element 22-7-24-21, and the physical covers 3_1, 5_3 and 7_2 of the physical element 3-21-24 are separately defined and have different degrees of freedoms, the discontinuity of the displacement jump over the interface 21-24 of the adjacent elements 22-7-24-21 and 3-21-24 can be easily captured while the mathematical mesh remain unchanged. This means in the NMM, the analysis of moving interface problems such as crack propagation and discontinuous deformation, can be performed until the end stages of failure, without the need for changing predefined mathematical mesh.

3 A simple and robust method for the generation of the finite covers

From the above introduction, it can be seen that, in the NMM, the mathematical mesh, ignoring the existence of physical lines is first constructed to define the interpolation accuracy, and the independent local cover functions are then defined at the physical covers which are obtained from the mathematical covers, as cut by the physical lines. It unifies the continuum analysis and discontinuum analysis without changing the predefined mathematical mesh, and has the advantages of being concise in theory as well as being clear in concept.

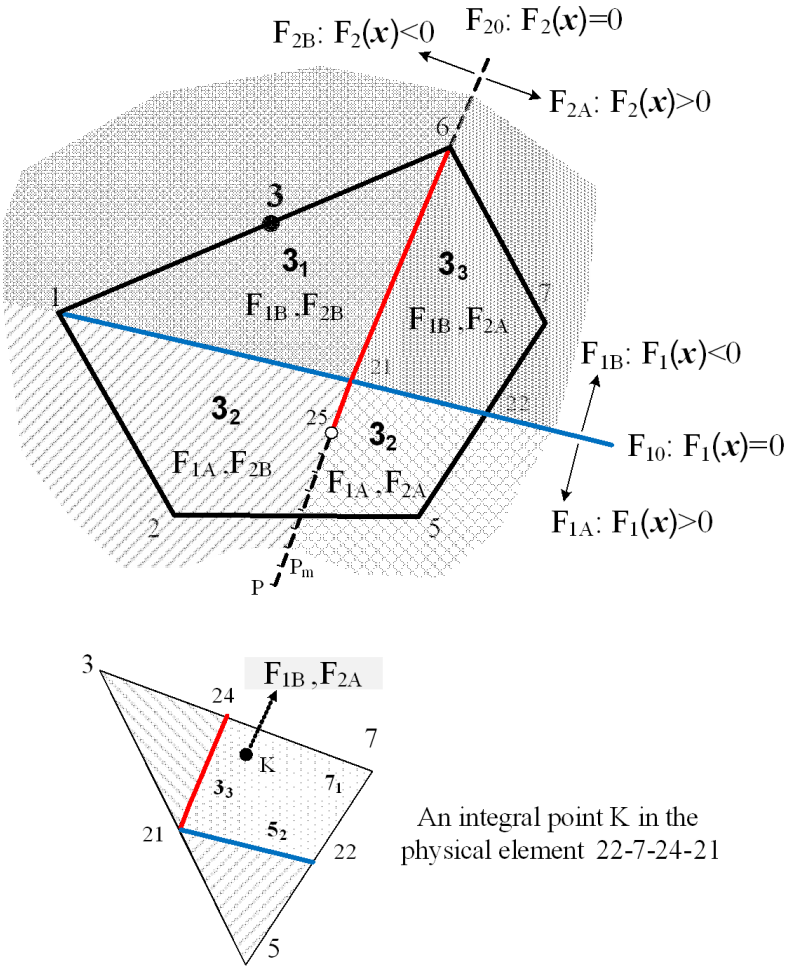

Figure 6: Generation of physical cover 3

A key and essential part in the implementation of the NMM is the generation of the finite covers, which includes the partitioning of independent physical covers and the indentification of the relations between physical covers and physical elements. For example, for the mathematical cover 3 in Fig.5, the simplest idea for the generation of the finite covers is to search out the closed regions 6-3-1-20-21-24, 1-2-5-22-21-20 and 22-7-6-24-21 by using the geometry algorithms, and record them as the independent physical covers 3_1, 3_2 and 3_3 respectively. Then the physical cover numbers of the physical element can be found out through the relative position between the integral points of the physical element and the physical covers. This method seems to be very simple, but actually it is quite difficult to be implemented in the NMM, due to the usage of the complex geometry algorithms and the time-consuming judgment of the point-polygon relations, especially for three dimensional analyses. Up to now, the absence of an effective cover generation theory is still the bottle neck of the research and application of the NMM.

In the following, a novel simple and robust cover generation method is developed to address the above-mentioned issue in the NMM. The algorithmic steps are:

(1) Take the mathematical cover 3 which is bounded by 1-2-5-7-6-3 (Fig.2). It can be easily found that the mathematical cover 3 is partitioned by the physical lines 1 and 2. We suppose that the physical line 1 is described by function $\mathrm{F}_1(\mathbf{x}) = 0$ and the physical line 2 is described by function $\mathrm{F}_2(\mathbf{x}) = 0$, denoted as F_{10} and F_{20} respectively. The physical line 1 partitions the mathematical cover 3 into two parts $\mathrm{F}_1(\mathbf{x}) > 0$ and $\mathrm{F}_1(\mathbf{x}) < 0$, denoted as $\mathrm{F}_{1\mathrm{A}}$ and $\mathrm{F}_{1\mathrm{B}}$ respectively. The physical line 2 partitions the mathematical cover 3 into two parts $\mathrm{F}_2(\mathbf{x}) > 0$and $\mathrm{F}_2(\mathbf{x}) < 0$, denoted as $\mathrm{F}_{2\mathrm{A}}$ and $\mathrm{F}_{2\mathrm{B}}$ respectively, as shown in Fig.6.

(2) Record the 2^ndifferent regions, which are obtained from the mathematical cover i partitioned by n physical lines, with a $2^n \times n$matrix $\mathbf{R}_i$. For example, the mathematical cover 3 in Fig.6 is partitioned into 4 regions by the physical lines 1 and 2, which can be recorded as

$$\mathbf{R}_i = \begin{bmatrix} \mathrm{F}_{1\mathrm{B}}, \mathrm{F}_{2\mathrm{B}} \\ \mathrm{F}_{1\mathrm{A}}, \mathrm{F}_{2\mathrm{B}} \\ \mathrm{F}_{1\mathrm{A}}, \mathrm{F}_{2\mathrm{A}} \\ \mathrm{F}_{1\mathrm{B}}, \mathrm{F}_{2\mathrm{A}} \end{bmatrix}$$

(3) The position of the tip point 25 of the physical line 1 falls into the interior of the mathematical cover 3. According to the definition of the physical covers, the regions $\left(\mathrm{F}_{1\mathrm{A}}, \mathrm{F}_{2\mathrm{B}}\right)$ and $\left(\mathrm{F}_{1\mathrm{A}}, \mathrm{F}_{2\mathrm{A}}\right)$ belong to a same physical cover 3_2 because $\left(\mathrm{F}_{1\mathrm{A}}, \mathrm{F}_{2\mathrm{B}}\right)$ and $\left(\mathrm{F}_{1\mathrm{A}}, \mathrm{F}_{2\mathrm{A}}\right)$ are not totally separated by the physical line and they don't have the independent deformations, as shown in Fig.6. To deal with this case automatically, we extend the tip point 25 to point P, where P should be outside of

the mathematical cover 3. Divide the line 25-P into m equal segments, e.g., $m = 10$ The divided points are denoted as P_m. Then we can compute and obtain the function values $\left(\mathrm{F}_{1\mathrm{A}}, \mathrm{F}_{20}\right)$ of the points P_m, where F_{20} indicates that the points P_m lie in the physical line 2. Set all the items related to the physical line 2 at the matrix $\mathbf{R}_i$ to 0, that is

$$\mathbf{R}_i\left(\mathrm{P}_m\right) = \begin{bmatrix} \mathrm{F}_{1\mathrm{B}}, 0 \\ \mathrm{F}_{1\mathrm{A}}, 0 \\ \mathrm{F}_{1\mathrm{A}}, 0 \\ \mathrm{F}_{1\mathrm{B}}, 0 \end{bmatrix}$$

We can see that the regions with the same item $\left(\mathrm{F}_{1\mathrm{A}}, 0\right)$ in the matrix $\mathbf{R}_i\left(\mathrm{P}_m\right)$ belong to a same physical cover. Thus, by comparing matrix $\mathbf{R}_i$ with matrix $\mathbf{R}_i\left(\mathrm{P}_m\right)$, it can be found that the regions $\left(\mathrm{F}_{1\mathrm{A}}, \mathrm{F}_{2\mathrm{B}}\right)$ and $\left(\mathrm{F}_{1\mathrm{A}}, \mathrm{F}_{2\mathrm{A}}\right)$ belong to a same physical cover 3_2. Note here that if the function values of the points P_m are all zero, that means the function values are represented by $\left(\mathrm{F}_{10}, \mathrm{F}_{20}\right)$, we don't need to perform this step for identifying the same physical cover.

(4) At this point, we have completed the generation of the independent physical covers for the mathematical cover 3. As shown in Fig.6, the mathematical cover 3 is partitioned into the independent physical covers 3_1, 3_2 and 3_3. The next step is to identify the physical cover numbers of the corresponding physical elements.

(5) For example, for an arbitrary integral point K at the physical element 22-7-24-21, we compute and obtain the function values $\left(\mathrm{F}_{1\mathrm{B}}, \mathrm{F}_{2\mathrm{A}}\right)$ of the point K by substituting the coordinates of the point K into the functions $\mathrm{F}_1(\mathbf{x})$ and $\mathrm{F}_2(\mathbf{x})$. It can be found that the integral point K belongs to the physical cover 3_3.

If we repeat the above described process, the finite covers over the entire domain can be easily generated. It can be seen that, the present method is simple and robust, and is also very fast because it avoids the usage of the complex geometry algorithm and the time-consuming judgment of the point-polygon relations, which are commonly used in the previous literatures. It is expected that the proposed theory and algorithms will contribute to be the basis for further research and application of the NMM.

It can be verified that the proposed method is suitable for the correct generation of various complex cases in which the mathematical cover is cut by multiple physical lines such as cracks. Let's check the special case in Fig.7, in which the mathematic cover 3 is partitioned into 4 different regions by two arbitrary physical lines

$F_1(\mathbf{x}) = 0$ and $F_2(\mathbf{x}) = 0$ as

$$\mathbf{R}_i = \begin{bmatrix} F_{1B}, F_{2B} \\ F_{1A}, F_{2B} \\ F_{1A}, F_{2A} \\ F_{1B}, F_{2A} \end{bmatrix}$$

By using the step 3 of the above described procedure, we find that (F_{1B}, F_{2B}) and (F_{1A}, F_{2B}) belong to a same physical cover 3_1. Furthermore, the region (F_{1A}, F_{2A}) is the invalid physical region because no integral point falls into the polygon of the mathematical cover 3 bounded by 1-2-5-7-6-3. Thus, the mathematical cover 3 is actually partitioned into two valid physical covers 3_1 and 3_2, as shown in Fig.7. However, we don't have to employ a special algorithm to find out the invalid physical regions in the implementation of the present method. It can be easily found that the invalid physical regions are the regions containing no integral points, when we complete the computing and assembling of the stiffness matrix of each integral point following the same procedure in the FEM. We can simply skip these invalid physical covers when numbering the degrees of freedom over physical covers.

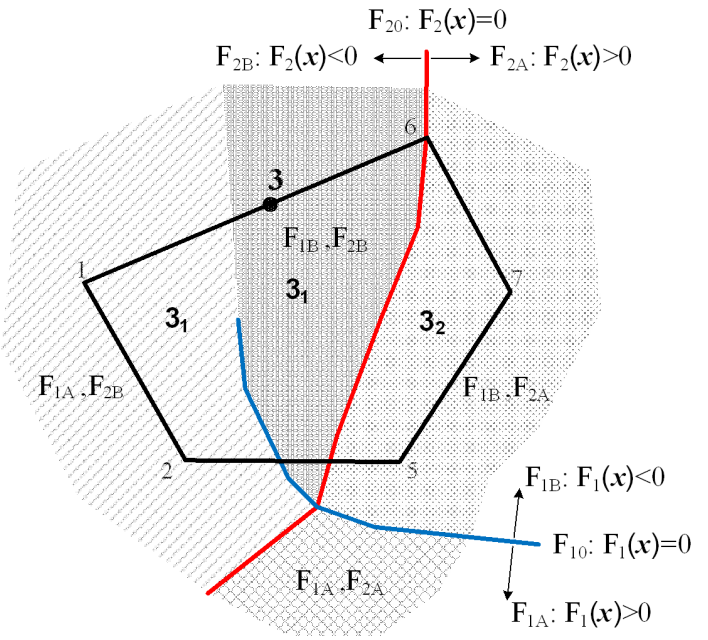

Figure 7: A special case of the generation of the physical cover

4 Numerical examples

4.1 Central-cracked plate

A plate with a central crack of length $2a$, as shown in Fig. 8 is firstly tested by the present method. The dimensions of the plate used in the test are L = 2m and W= 1m. The plate is subjected to uniform traction of σ = 3MPa in y direction. The elastic material parameters used are $E = 3.0\times10^4$MPa and $\upsilon = 0.3$. The problem is solved under plane stress assumption. A number of tests have been performed by varying a between $0.2W$, $0.4W$ and $0.6W$. The problem is modeled using 448 and 1416 irregular nodes and solved for plane stress case. The analytical solution for K_I is available in Anderson (1995) as

$$K_I = \sigma\sqrt{\pi a}\sqrt{\sec\frac{\pi a}{2W}}\left[1-0.025\left(\frac{a}{W}\right)^2+0.06\left(\frac{a}{W}\right)^4\right] \tag{6}$$

The computational results of the SIFs by the NMM are listed in Table 1. Table 1 indicates that the NMM solution is in a good agreement with the analytical solution even for sparsely distributed nodes.

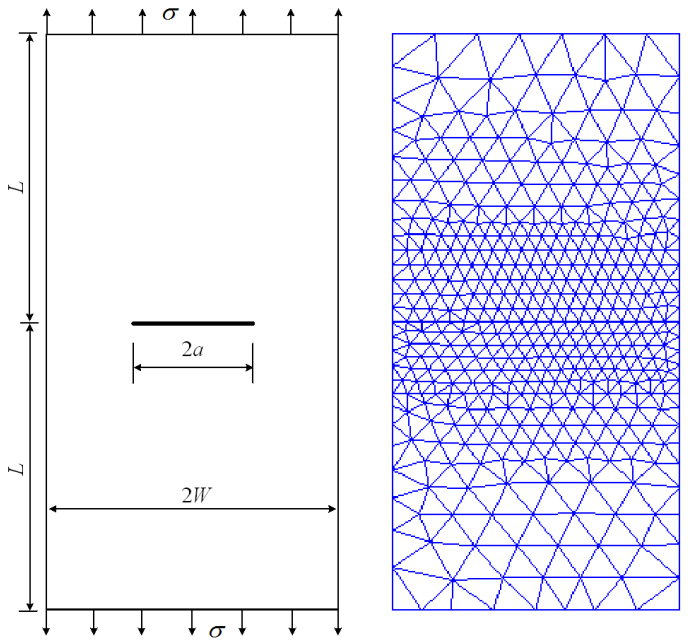

Figure 8: Central-cracked plate

Table 1: SIFs for the central-cracked plate

a/W	448 nodes		1416 nodes		Analytical
	K_I	Error	K_I	Error	
0.2	2.4150	-0.87%	2.4313	-0.20%	2.4362
0.4	3.6638	-1.77%	3.6863	-1.16%	3.7297
0.6	5.2837	-1.53%	5.2952	-1.32%	5.3658

4.2 Three-point bend specimen

The problem of a stationary crack in a three-point bend specimen is considered. The geometry is shown in Fig. 9. The crack is located at the midspan of the beam so that only mode I cracking develops. The dimensions of the specimen are $S = 12$ and $W = 6$. The load is $F = 1$ applied over unit length and unit depth. The discretisation with 1977 nodes is also shown in Fig. 9 and the computed SIFs are compared with the analytical solution obtained by John (1976) in Table 2. As can be seen from the table, the NMM shows high solution accuracy for SIFs with the maximum error less than 1.61%.

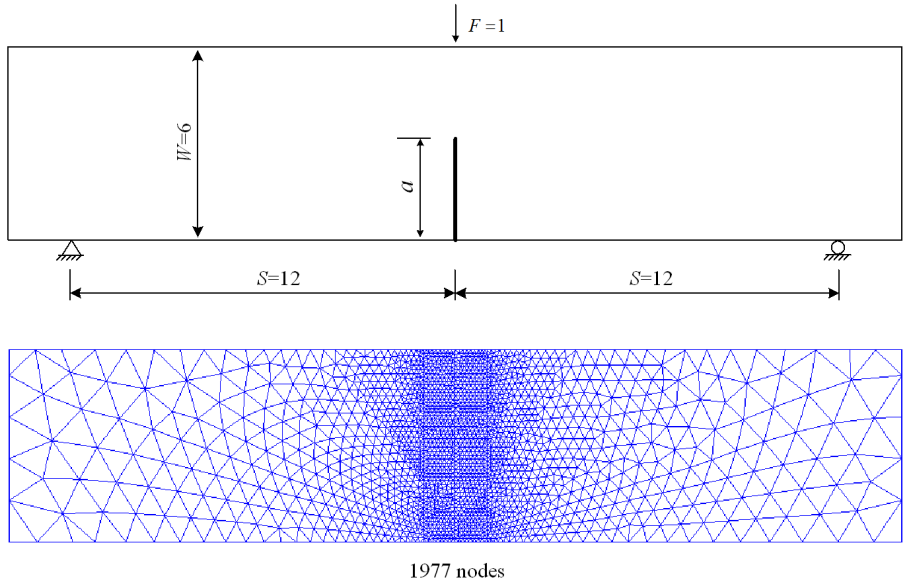

Figure 9: A three-point bending specimen

Table 2: SIFs for the three-point bend specimen

a/W	0.3		0.4		0.5	
	K_I	Error	K_I	Error	K_I	Error
Reference	2.484	–	3.236	–	4.348	–
Present	2.444	-1.61%	3.256	0.62%	4.305	-0.99%

4.3 Curved crack in an infinite plate

The problem of a curved crack in an infinite plate is considered. The dimensions of the model are shown in Fig.10, with$R = 4.25$ and $\beta = 28.0725°$. The analytical solutions for SIFs of the problem are available in Gdoutos (1979) and Budyn(2004).

The discrete model with 2083 nodes is shown in Fig.11. The comparison of the SIF results from the NMM and the analytical solutions is listed in Table 3. It is seen that the NMM shows good accuracy for this problem.

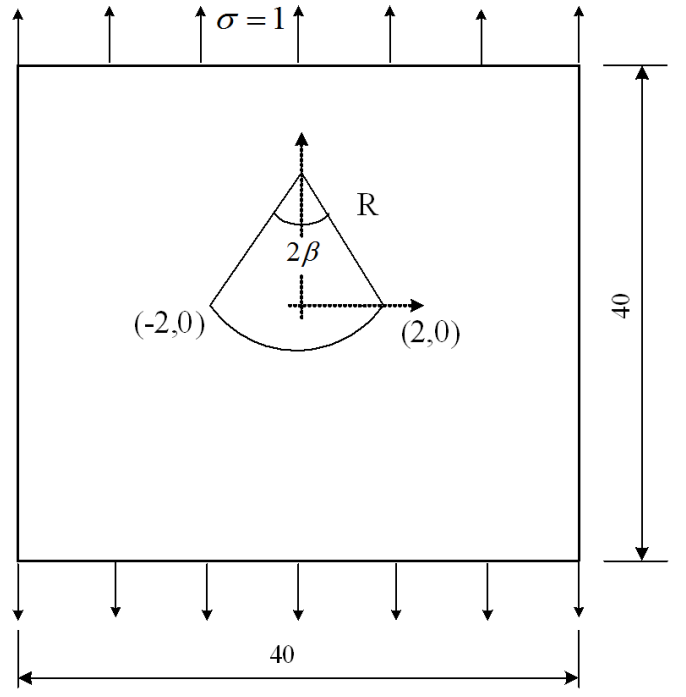

Figure 10: Curved crack in an infinite plate

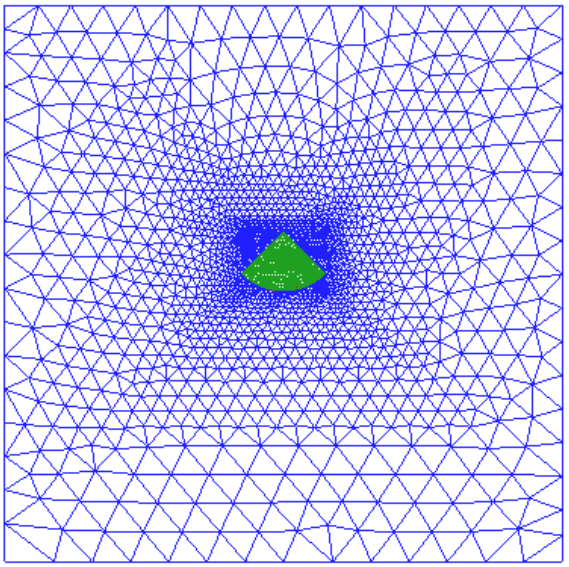

Figure 11: 2083 discrete nodes

Table 3: SIFs for the curved crack

	Present	Analytical	Error
K_I	2.026	2.015	0.55%
K_{II}	1.138	1.112	2.34%

4.4 Branched crack in an infinite plate

A branched crack in an infinite plate under uniform tension is examined as shown in Fig.12. The dimensions of the model are fixed to $H = 4$, $W = 5$, $a/W = 0.05$, $b/a = 0.9$ and $\theta = 45^0$. The material constants are the Young's modulus $E = 1000$ and the Poisson's ration $v = 0.3$. Totally 3678 discrete nodes were used for discretisation as shown in Fig. 13. The normalized stress intensity factors for tips A and B are defined as

$$F_I^A = K_I^A/\sigma\sqrt{\pi c}, F_I^B = K_I^B/\sigma\sqrt{\pi c}, F_{II}^B = K_{II}^B/\sigma\sqrt{\pi c}$$

where $c = (a + b\cos\theta)/2$.

The SIF results from the NMM and the reference solution (Chen and Hasebe 1995) are listed in Table 4. It is seen that the relative error is less than 1.06% for all the cases.

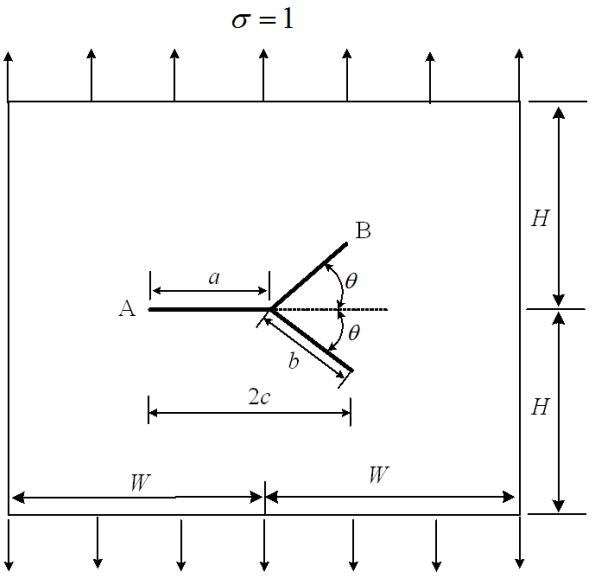

Figure 12: Branched crack in an infinite plate

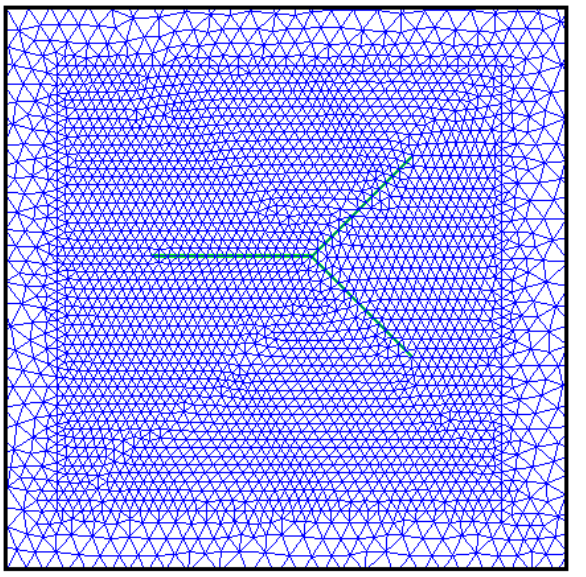

Figure 13: Discrete nodes for branched crack

Table 4: SIFs for branched crack in an infinite plate

	Present	Analytical	Error
F_I^A	1.029	1.040	-1.06%
F_I^B	0.492	0.495	-0.61%
F_{II}^B	0.501	0.503	-0.40%

4.5 An embedded star-shaped crack

In this example, we considered a star-shaped crack as shown in Fig.14. The geometrical parameters are $\theta = 60^0$, $W = 4$ and $a/W = 0.05$. Uniform stress $\sigma = 50$ is applied to each edge. The mesh used in NMM with 2844 nodes is shown in Fig.15. F_{1A} and F_{1A} in Table 5 are defined as

$$F_{1A} = K_{1A}/\sigma\sqrt{\pi a} \quad , \quad F_{1B} = K_{1B}/\sigma\sqrt{\pi a}$$

It is seen that the SIF results listed in Table 5 are in good agreement with Chen and Hasebe (1995).

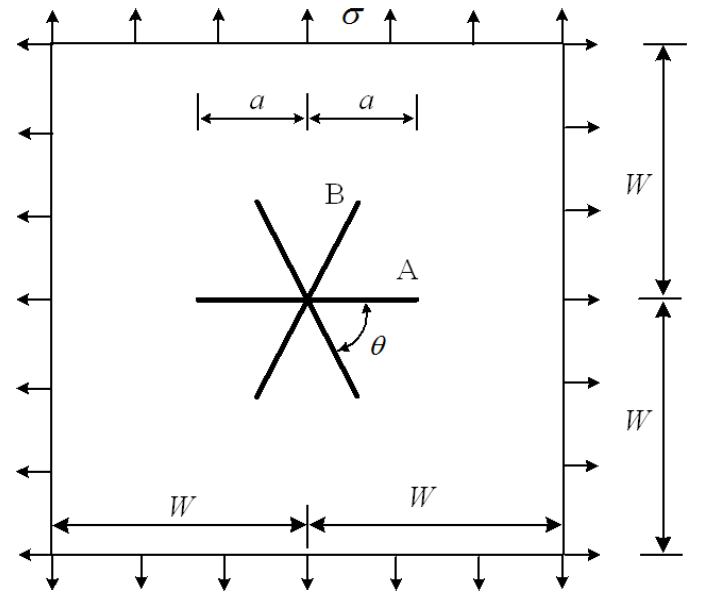

Figure 14: An embedded star-shaped crack

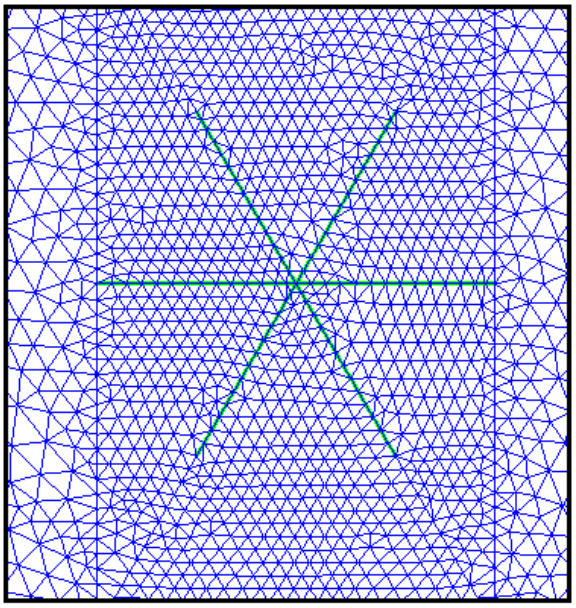

Figure 15: Discrete nodes for star-shaped crack

Table 5: SIFs for star-shaped crack

	Present	Analytical	Error
F_I^A	0.744	0.743	0.13%
F_I^B	0.749	0.743	-0.81%

5 Conclusions

In this paper, a new method is proposed for the automatic generation of the finite covers in the NMM for the modeling of cracks. The present method of cover generation is simple and robust, and is also very fast because it avoids the usage of the complex geometry algorithm and the time-consuming judgment of the point-polygon relations. It is expected that the proposed theory and algorithms will contribute to be the basis for further research and application of the NMM.

Only two-dimensional stationary elastic fracture problems are investigated and discussed in this paper. Extensions of the present work to the crack growth simulation and three dimensional analyses are natural and feasible. They will also be the further work of the present authors.

Acknowledgements

The authors gratefully acknowledge the support of National Basic Research Program of China (973 Program: 2011CB013800), New Century Excellent Talents Project in China (NCET-12-0415), Program for Changjiang Scholars and Innovative Research Team in University (PCSIRT, IRT1029), and Fundamental Research Funds for the Central Universities.

References

An, X. M.; Fu, G.Y.; Ma, G.W. (2012): A comparison between the NMM and the XFEM in discontinuity modeling *International Journal of Computational Methods*, vol. 9, issue 2 DOI: 10.1142/S0219876212400300.

An, X.M.; Ma, G.W.; Cai, Y.C.; Zhu, H.H. (2011a): A new way to treat material discontinuities in the numerical manifold method. *Computer Methods in Applied Mechanics and Engineering*, vol.20, pp. 3296-3308.

An, X.M.; Ma, G.W.; Cai, Y.C; Zhu, H.H. (2011b): Arbitrary discontinuities in the numerical manifold method. *International Journal of Computational Methods*, vol. 8, pp. 315-347.

Anderson, T.L.(1995): Fracture mechanics: foundamentals and application. 2^{nd} Edition. *Boca Raton:CRC*.

Atluri, S. N. (1998): Structural Integrity and Durability, *Forsyth*: *Tech Science Press*.

Atluri, S.N. (2005): Methods of computer modeling in engineering and the sciences. *Tech Science Press*.

Atluri, S. N.; Kobayashi, A. S.; Nakagaki M. (1975): An assumed displacement hybrid finite element model for linear fracture mechanics, *International Journal of Fracture*, vol. 11, no. 2, pp. 257-271.

Barsoum, R. S. (1976): On the use of isoparametric finite elements in linear fracture mechanics. *International Journal for Numerical Methods in Engineering*, Vol.10, issue 1, pp. 25-37.

Belytschko T.; Fleming M.(1999): Smoothing, enrichment and contact in the element-free Galerkin method. Computers and Structures, vol. 71, pp.173-195.

Budyn, E.R.L.(2004): Mutiple crack growth by the extended finite element method. *Northwestern University*.

Cai, Y.C.; Zhuang X.Y.; Zhu, H.H.(2013): A generalized and efficient method for finite cover generation in the numerical manifold method. *International Journal of Computational Methods*, vol.10, DOI: 10.1142/S021987621350028X.

Chen Y.; Hasebe N(1995): New integration scheme for the branch crack problem. *Engineering Fracture Mechanics*, vol. 52, pp.791801.

Ching H.-K.; Batra R. C.(2001): Determination of crack tip fields in linear elastostatics by the Meshless Local Petrov-Galerkin (MLPG) method. *CMES: Computer Modeling in Engineering & Sciences*, vol. 2, no. 2, pp. 273-290.

Dong, L.; Atluri, S. N. (2012): SGBEM (using non-hyper-singular traction BIE), and super elements, for non-collinear fatigue-growth analyses of cracks in stiffened panels with composite-patch repairs. *CMES: Computer Modeling in Engineering & Sciences*, vol.89, no.5, pp.417-458.

Dong, L.; Atluri, S.N. (2013a): Fracture & fatigue analyses: SGBEM-FEM or XFEM? Part 1: 2D structures. *CMES: Computer Modeling in Engineering & Sciences*, vol.90, no.2, pp. 91-146.

Dong, L.; Atluri, S.N. (2013b): Fracture & fatigue analyses: SGBEM-FEM or XFEM? Part 2: 3D solids. *CMES: Computer Modeling in Engineering & Sciences*, vol.90, no.5, pp 379-413.

Fleming, M.;Chu,Y.A.;Moran, B.;Belytschko, T.(1997): Enriched element-free Galerkin methods for crack tip fields. *International journal for numerical methods in engineering*, vol.40, pp.1483-1504.

Gdoutos, E.(1979): Fracture mechanics. *Boston:Kluver Academics Publisher*.

Gu, YT.; Wang W.; Zhang LC.; Feng XQ.(2011): An enriched radial point interpolation method (e-RPIM) for analysis of crack tip fields. *Engineering Fracture Mechanics*, vol.78, pp.175–190.

Han, Z. D.; Atluri, S. N. (2002): SGBEM (for Cracked Local Subdomain) – FEM (for uncracked global Structure) alternating method for analyzing 3D surface cracks and their fatigue-growth. *CMES: Computer Modeling in Engineering & Sciences,* vol.3, no.6, pp.699-716.

Han, Z. D.; Atluri, S. N. (2003): On simple formulations of weakly-singular traction & displacement BIE, and their solutions through Petrov-Galerkin approaches. *CMES: Computer Modeling in Engineering & Sciences*, vol.4, no.1, pp.5-20.

Henshell, R. D.; Shaw, K. G. (1975): Crack tip finite elements are unnecessary. *International Journal for Numerical Methods in Engineering*, vol. 9, issue 3, pp.495-507.

Jiang, Q.H.; Zhou, C.B; and Li, D.Q. (2009): A three-dimensional numerical manifold method based on tetrahedral meshes. *Computers & Structures*, vol. 87, pp. 880-889.

John ES.(1976): Wide range stress intensity factor expressions for ASTM E399 standard fracture toughness specimens. *International Journal of Fracture*, vol.12,

pp.475-476.

Liu, Y.R.; Chang, Q.; Yang, Q.; Wang, C.Q.; Guan, F.H. (2011): Fracture analysis of rock mass based on 3-D nonlinear Finite Element Method. *Science China-Technological Sciences*, vol. 54, pp. 556-564.

Ma, G.W.; An, X.M.; Zhang, H.H.; Li, L.X. (2009). Modeling complex crack problems with numerical manifold method. *International Journal of Fracture*, vol. 156, pp. 21-35.

Ma, G.W.; An, X.M.; He, L. (2010): The numerical manifold method: a review. *International Journal of Computational Methods*, vol. 7, pp. 1-32.

Melenk J M; Babuska I. (1996): The partition of unity finite element method: basic theory and applications *Computer Methods in Applied Mechanics and Engineering*, vol. 39, pp. 289–314.

Moes N.; Dolbow, J. O. H. N.; Belytschko, T. (1999): A finite element method for crack growth without remeshing. *International journal for numerical methods in engineering*, vol. 46, no.1, pp. 131-150.

Nikishkov, G. P.; Park, J. H.; Atluri, S. N. (2001): SGBEM-FEM alternating method for analyzing 3D non-planar cracks and their growth in structural components. *CMES: Computer Modeling in Engineering & Sciences*, vol.2, no.3, pp.401-422.

Ning, Y.J.; An, X.M.; Ma, G.W. (2011): Footwall slope stability analysis with the numerical manifold method. *International Journal of Rock Mechanics & Mining Sciences*, vol.48, pp. 964-975.

Shi, G.H. (1991): Manifold method of material analysis. Trans. 9th Army Conf. Applied Mathematics and Computing, Minneapolis, Minnesota pp. 57-76.

Shi, G.H. (1992): Modeling rock joints and blocks by manifold method. Rock Mech. Proc. 33rd U. S. Symposium, Santa Fe, New Mexico, pp. 639-648.

Sukumar, N.; Chopp, D. L.; Moes, N., Belytschko, T. (2001): Modeling holes and inclusions by level sets in the extended finite-element method. *Computer methods in applied mechanics and engineering*, vol. 190, no. 46, pp. 6183-6200.

Sukumar, N.; Chopp, D. L.; Béchet, E.; Moës, N. (2008): Three-dimensional non-planar crack growth by a coupled extended finite element and fast marching method. *International journal for numerical methods in engineering*, vol. 76,issue 5, pp. 727-748.

Terada, K.; Kurumatani, M. (2005): An integrated procedure for three-dimensional structural analysis with the finite cover method. *International Journal for Numerical Methods in Engineering*, vol. 63, pp. 2102-2123.

Tong, P; Pian T. H. H; Lasry S. J. (1973): A hybrid-element approach to crack

problems in plane elasticity. *International Journal for Numerical Methods in Engineering*, vol. 7, issue 3, pp. 297-308.

Wu,Z.J.; Wong, L.N.Y.(2012): Frictional crack initiation and propagation analysis using the numerical manifold method. *Computers and Geotechnics*, vol.39, pp.38-53.

Xu, Y.; Saigal S.(1998): An element free Galerkin formulation for stable crack growth in an elastic solid. *Computer Methods in Applied Mechanics and Engineering*, vol.154, pp.331-343.

Zhang, H.H.; Li, L.X.; An, X.M.; Ma, G.W. (2010): Numerical analysis of 2-D crack propagation problems using the numerical manifold method. *Engineering Analysis with Boundary Elements*, vol. 34, pp.41-50.

Zhang, Z.R.; Zhang, X.W.; Yan, J.H. (2010): Manifold method coupled velocity and pressure for Navier-Stokes equations and direct numerical solution of unsteady incompressible viscous flow. *Computers & Fluids*, vol. 39, pp. 1353-1365.